

# Tension-based Multi-stable Compliant Rolling-contact Elements

Peter A. Halverson<sup>1</sup>, Larry L. Howell<sup>1\*</sup>, Spencer P. Magleby<sup>1</sup>

<sup>1</sup> Department of Mechanical Engineering, Brigham Young University, Provo, Ut, USA

\* corresponding author (email: lhowell@byu.edu)

## Abstract

This paper presents models for a tension-based, multi-stable, large displacement, compliant rolling-contact element (CORE). The models are capable of determining stress, strain, and retaining forces and are derived using a strain-energy approach. Models are compared to empirical results and the utility of these models is demonstrated in a case study. The case study demonstrates a device with multiple stable equilibrium positions and tests the fatigue properties of tension-stable CORE.

## 1 Introduction

Traditional pin-in-hole type hinges permit relative rotation between two rigid bodies. These mechanisms require clearance between the pin and the hole, introducing undesirable motions into the system. These motions can create problems with both precision and accuracy. The problems are compounded after time as the pin slides in the hole producing wear, thus increasing the clearance and further augmenting the problem. Compliant mechanisms have the potential to eliminate both friction and wear by achieving relative motion through the deflection of one or more of its members [1].

Because of their potential to alleviate problems with undesirable motion and wear, much research has been conducted into large displacement compliant revolute joints. Trease et al. [2] introduced a design criterion for various large-displacement compliant joints. The criterion stated that the joint must provide (1) a large range of motion, (2) minimal “axis drift” (3) increased off-axis stiffness, and (4) an avoidance of stress concentrations. COMpliant Rolling-contact Elements (CORE), such as the one shown in Figure 1, have been shown to fulfill this criterion [3, 4]. Other authors have referred to similar devices as rolamite hinges or Xr-joints [4–6]. CORE mechanisms reduce wear and friction by allowing the surfaces to roll on each other. Furthermore, CORE mechanisms eliminate high stress concentrations and resist both off-axis and compressive forces that present difficulties in many large-angle compliant joints. This is done by constraining the radius of the flexible segment, thus constraining the stress [3, 4, 7]. CORE mechanisms are similar to contact-aided compliant mechanisms, but with continuous rather than intermittent contact [8–10].

These advantages have led to new applications and increased study of CORE devices. In 1969 Donald Wilkes

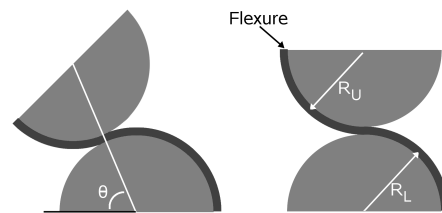


Figure 1: Movement of CORE (flexure thickness exaggerated for illustration purposes)

demonstrated that a “roller-band device”, capable of linear displacement, could be manufactured as to have a band-generated force [5]. This band-generated force was generated by varying the cross section of the roller-band. In 1974 Hilberry et al. [6] patented a CORE mechanism for use as an artificial knee. The shape of the constraining surface was used to generate a restoring moment. Equations governing this phenomenon were not disclosed. Other researchers have demonstrated additional methods of force generation [11]. A recent paper identified seven concepts that, when applied to a CORE, produced multiple stable positions in which an external force was not required to maintain the current position (multi-stability) [12]. These positions corresponded to local minima in potential energy.

This paper contributes to the area of multi-stable CORE by presenting models for stress, stabilizing torque, and stored potential energy for Tension-stable CORE, and illustrates how they can be used to create devices with multiple stable equilibrium positions. In addition, we examine a case study into the miniaturization of CORE and examine its fatigue properties.

Tension-stable CORE mechanisms can be constructed of three CORE planes and two cam and follower planes. Each CORE plane consists of two rigid, curved surfaces which roll on each other. A flexure joins the two surfaces together and when assembled is placed between the surfaces (see Figure 2). The CORE planes are then joined in alternating directions to insure that the surfaces stay in contact with the cam and follower planes, as illustrated in Figures 3 and 4. The

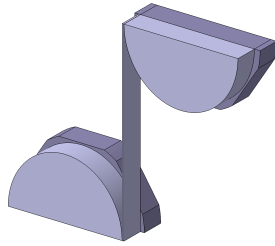


Figure 2: An unfolded CORE plane (foreground) with cam (background)

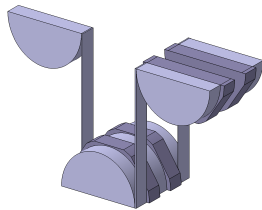


Figure 3: Unfolded CORE mechanism

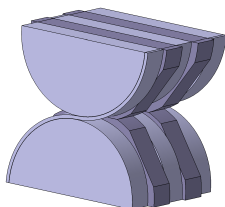


Figure 4: Assembled CORE mechanism

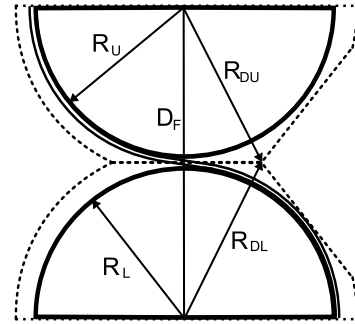


Figure 5: CORE mechanism in “inactive” position

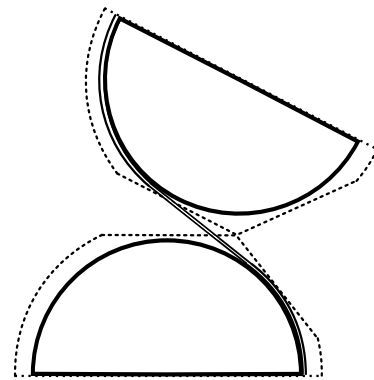


Figure 6: CORE mechanism in “active” position

flexure is fastened such that it insures a no-slip condition, much like the teeth on gears.

## 2 Guidelines for Cam Design

When the cam is not engaged, the compliant flexure is transferred from one surface to the other and assumes the curvature of the mating surface, as shown in Figure 5. While the cam is in the “inactive” position(s) it behaves as a standard CORE mechanism and will exhibit neutral stability, assuming an initially straight beam and that the upper and lower CORE surfaces are of the same radius (i.e.  $R_U = R_L$ ). As the CORE mechanism is displaced and the cam is engaged, the CORE surface separates; placing the flexure in tension as illustrated in Figure 6.

Consider the exaggerated CORE shown in Figure 7. If the foci,  $F_U$  and  $F_L$ , are considered pinned to ground it becomes apparent that

$$\omega_U R_{DU} = V_1 = \omega_L R_{DL} \quad (1)$$

where  $R_{DU}$  and  $R_{DL}$  are the distances from the contacting cam surface to the upper and lower CORE foci, and  $\omega_U$  and  $\omega_L$  are the angular velocities of the upper and lower surfaces

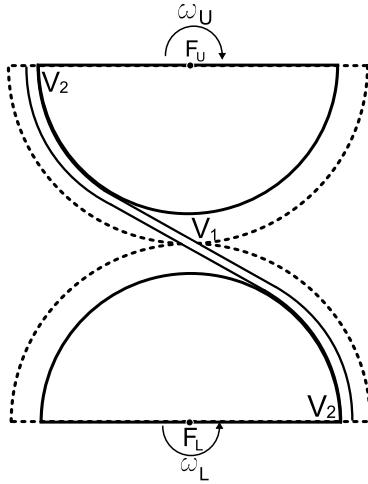


Figure 7: Velocity profiles of CORE (Cam surfaces exaggerated for illustration)

respectively and  $V_1$  is the tangential velocity at the contacting point. As the cam and the CORE surface have the same angular velocity, a theoretical no-slip condition holds when the connected CORE surfaces and the contacting cams have the same tangential velocity (Figure 7).

The relationship between the upper and lower cam radius and the upper and lower CORE surface radius is then expressed as

$$\frac{R_U}{R_L} = \frac{R_{DU}}{R_{DL}} \quad (2)$$

Some slip will occur as the flexure does not create a perfectly rigid connection between the CORE surfaces. This effect is examined more in detail later.

### 3 Modeling

When the cam is fully engaged, the distance between the two foci,  $D_F$  (see Figure 8), may be determined through the law of cosines as

$$D_F = \sqrt{R_{DL}^2 + R_{DU}^2 - 2(R_{DU})(R_{DL}) \times \cos(\theta_{DF})} \quad (3)$$

where the angle  $\theta_{DF}$ , the angle between the sides  $R_{DL}$  and  $R_{DU}$ , is defined by

$$\theta_{DF} = 180 - \theta_{R_{DU}} - \sin^{-1} \left( \frac{R_{DL}}{R_{DU}} \sin(\theta_{R_{DU}}) \right) \quad (4)$$

and  $\theta_{R_{DU}}$  is opposite of  $R_{DU}$  and is prescribed by

$$\theta_{R_{DU}} = \cos^{-1} \left( \frac{(R_U + R_L + h)^2 + R_{DL}^2 - R_{DU}^2}{2 \times (R_U + R_L + h)R_{DL}} \right) - \theta_1 \quad (5)$$

where  $\theta_1$  is the angle of rotation relative to the vertical axis. Due to its compliance, the flexible segment leaves both

CORE surfaces in a tangential direction. The length of the flexure that is straight,  $L_S$ , may be calculated as

$$L_S = (R_U + R_L) \sqrt{\left( \frac{D_F}{R_U + R_L} \right)^2 - 1} \quad (6)$$

The elongation that the flexure undergoes,  $E_L$ , is

$$E_L = L_S - (R_U + R_L) \cos^{-1} \left( \frac{R_U + R_L}{D_F} \right) \quad (7)$$

or

$$E_L = (R_U + R_L) \left[ \sqrt{\left( \frac{D_F}{R_U + R_L} \right)^2 - 1} - \cos^{-1} \left( \frac{R_U + R_L}{D_F} \right) \right] \quad (8)$$

and the strain,  $\epsilon$ , is

$$\epsilon = \frac{E_L}{L_i} \quad (9)$$

where  $L_i$  is the initial length of the flexure. The strain energy of the system is expressed as

$$U = \frac{F^2 L_i}{2AE} \quad (10)$$

### 3.1 Stress Analysis

The stress due to tension,  $\sigma_T$ , is

$$\sigma_T = E\epsilon \quad (11)$$

where  $E$  is the modulus of elasticity. The stress due to bending,  $\sigma_B$ , is calculated as

$$\sigma_B = \frac{Eh}{2R_S} \quad (12)$$

where  $h$  is the cross-sectional thickness.

### 3.2 Retaining Forces

The force generated in one flexure,  $F$ , is calculated from the stress as

$$F = \sigma_T A \quad (13)$$

where  $A$  is the cross-sectional area. Once the stress is known, the retaining forces may be calculated using the free-body diagram shown in Figure 8, where

$$\theta_c = \sin \left( \frac{L_S}{D_F} \right) \quad (14)$$

The moment about the contact point is calculated for a flexure that is wrapped counter-clockwise and clockwise around the upper surface by constructing a new axis  $x'y'$  about the contact point. The location where the flexible segment leaves the CORE surface on the  $x'y'$  coordinate system is then determined by

$$A_{x'} = R_{DU} - R_U \cos(\theta_{R_{DL}} + \theta_C) \quad (15)$$

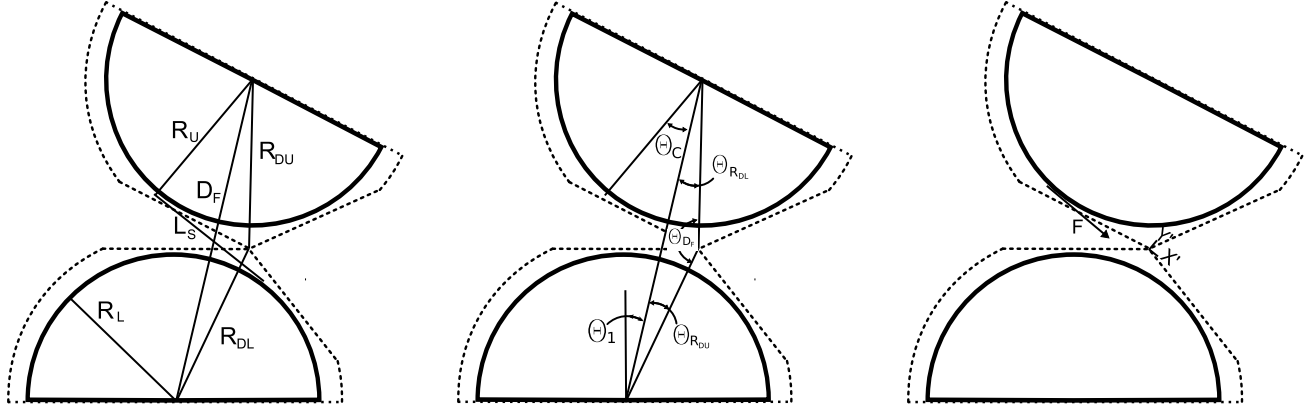


Figure 8: Referenced lines (left), angles (center), and forces (right) for tension-stable CORE

where  $\theta_{RDL}$  is the angle prescribed by

$$\theta_{RDL} = 180 - \theta_{DF} - \theta_{RDU} \quad (16)$$

$$A_{y'} = R_U \sin(\theta_{RDL} + \theta_C) \quad (17)$$

The  $x'$  and  $y'$  of components of the force,  $F_{x'}$  and  $F_{y'}$  are

$$F_{x'} = -F \cos(\theta_{RDL} + \theta_C) \quad (18)$$

$$F_{y'} = -F \sin(\theta_{RDL} + \theta_C) \quad (19)$$

Thus the overall moment about the contacting point, due to the counter-clockwise wrapped flexure,  $M_{ccw}$ , is

$$M_{ccw} = -(R_{DU} - R_U \cos(\theta_{RDL} + \theta_C)) \times F \sin(\theta_{RDL} + \theta_C) - R_U \sin(\theta_{RDL} + \theta_C) \times F \cos(\theta_{RDL} + \theta_C) \quad (20)$$

Likewise the effect of the beams wound clockwise around the upper CORE surface can be found by

$$A_{x'} = R_{DU} - R_U \cos(\theta_{RDL} - \theta_C) \quad (21)$$

$$A_{y'} = R_U \sin(\theta_{RDL} - \theta_C) \quad (22)$$

The  $x'$  and  $y'$  of components of the force are

$$F_{x'} = -F \cos(\theta_{RDL} - \theta_C) \quad (23)$$

$$F_{y'} = -F \sin(\theta_{RDL} - \theta_C) \quad (24)$$

Thus the overall moment about the contacting point, due to the clockwise wrapped flexure,  $M_{cw}$  is

$$M_{cw} = -(R_{DU} - R_U \cos(\theta_{RDL} - \theta_C)) \times F \sin(\theta_{RDL} - \theta_C) - R_U \sin(\theta_{RDL} - \theta_C) \times F \cos(\theta_{RDL} - \theta_C) \quad (25)$$

And the total overall moment is simply the sum of  $M_{cw}$  and  $M_{ccw}$ . The unstable equilibrium point occurs when  $\theta_c = 0$ .

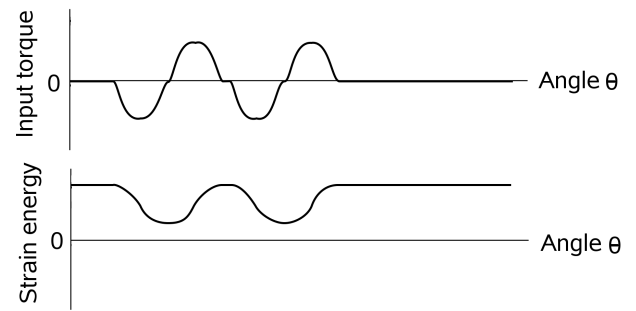


Figure 9: Potential energy of bistable CORE

### 3.3 Stability

The potential energy, due to tension, of the system may then be determined by combining equations (10), (11), and (13).

$$U = \frac{EAE_L^2}{2L_i} \quad (26)$$

A graph illustrating the potential energy curve of a bistable mechanism is shown in Figure 9. Local minimums of potential energy represent stable equilibrium positions, and the tension-stable CORE mechanism can be designed to have multiple stable equilibrium positions. An example of a device with multiple stable equilibrium positions is demonstrated in the next section

## 4 Case Study

The utility of the models derived above may be illustrated by a case study. A hinge of a small device capable of folding, as shown in Figure 10, is used as the case study for this research. The device requires (1) a thickness, of less than 10 mm, (2) a holding force, or the force that prevents the device from opening, of about 1.5 N, (3) a retaining force, or the force that prevents the device from closing, of about 2-3 N, and (4) stable position when closed and when opened to 150 degrees. In addition, the hinge needs to be designed for a

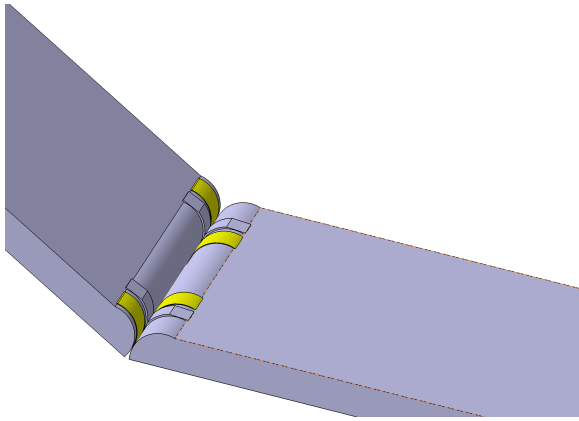


Figure 10: Small device case study showing a hinge for folding

Table 1: Material comparison showing stresses for a 10mm CORE hinge

Material	$\sigma_B$ (MPa)	$\sigma_T$ (MPa)	$\sigma_{Total}$ (MPa)
Steel	379	447	826
Aluminum	186	250	435
Titanium	216	363	579
Kevlar 29	3	278	281
Kevlar 49	3	317	320

fatigue life of at least 100,000 cycles to insure that the hinge would outlast the life of the device. Other constraints included symmetry of CORE surfaces and a small part count.

In order to determine the minimum size of the hinge, an optimization routine was implemented via OptdesX, using the above equations. The holding force was considered the tangential force located on the end of the device. The center of gravity, was considered to act on the midpoint of the device. Thus the input force,  $F_{in}$  was calculated as follows

$$F_{in} = \frac{M_{ccw} + M_{cw}}{L} - \frac{1}{2} \cos(\theta)W \quad (27)$$

where  $L$  and  $W$  are the length and weight of the device. As material selection for the flexure was key, several traditional metals were investigated as well as several polymers, and composite materials. The stresses for a 10mm (6.7 mm radius) CORE hinge that meets the above requirements are listed in Table 1. It is interesting to note that, due to the low modulus of elasticity of ABS, a hinge could not be constructed that fit all 4 requirements.

High bending stresses are expected for metals due to their high stiffness. As bending stresses do not contribute to the overall stability of tension-stable CORE, anisotropic fibrous materials, such as Kevlar have been investigated. Ultimately Kevlar 49 was chosen for the construction of the physical prototype and fatigue testing due to its excellent creep resistant properties and low flexural modulus.

The mechanism was prototyped using a CNC mill to the

Table 2: Specifications of CORE hinge

Specification	Value
Core Surface Radius	3.5 mm
Cam radius	3.71 mm
Flexure area	$4.4 * 10^{-7} \text{ mm}^2$
Flexure length	1.6 mm
Unstable equilibrium Angle	$29.5^\circ$

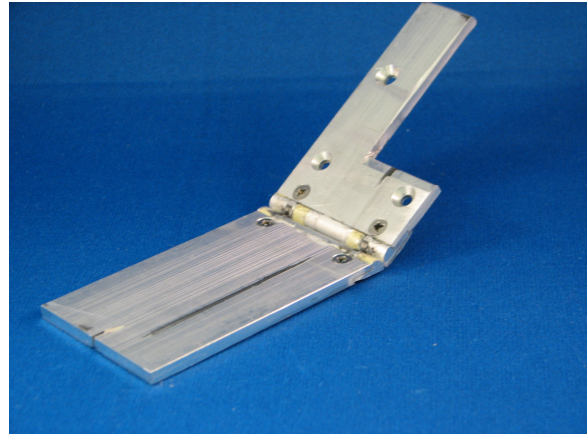


Figure 11: Example of the prototyped device used for testing.

specifications listed in Table 2 and is shown in Figure 11. The unstable equilibrium angle is the angle at which  $F_{in}$  becomes negative, or in other words the angle when the device will open unassisted.

#### 4.1 Assembly

As Kevlar's chemical composition makes it difficult to bond to metals, a clamping mechanism was employed. The fibers were laid over half the CORE mechanism and a small amount of epoxy (methyl-2-cyanoacrylate) was applied, as a secondary method of securing the fibers, to the mechanism just behind the CORE Surface. The remaining half of the mechanism was lowered into place, clamping the fibers to the other half. This piece was secured via 2 screws as shown Figure 12.

The fibers were trimmed after assembly to avoid protrusions. This half of the mechanism was then placed into a



Figure 12: Demonstration of clamping method used to secure the Kevlar fibers

Table 3: Empirical and analytical comparison

Metric	Predicted	Actual	Error
Maximum torque	0.122 N/m	0.118 N/m	3.2 %
Maximum torque angle	11°	11.727°	6.6%
Unstable Equilibrium Angle	29.5°	30.5°	3.4%

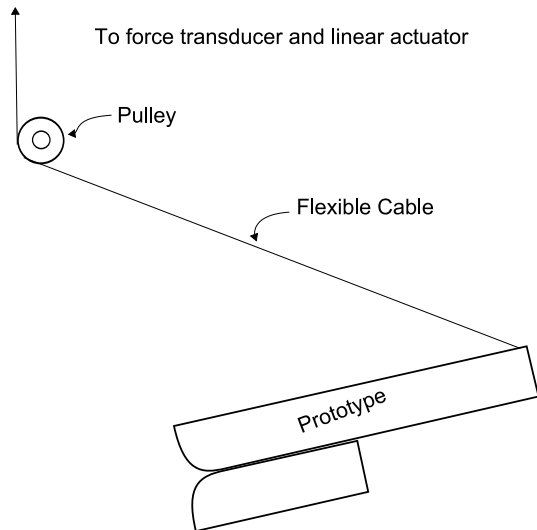


Figure 13: Schematic of force measurement setup

jig and assembled in the 150° position. During the manufacturing of the device care was taken to remove any surfaces that could damage the Kevlar, such as sharp edges and burrs. Lastly, before the Kevlar was clamped into the mechanism, a small amount of methyl-2-cyanoacrylate was applied to the fibers, further securing the fibers in place.

## 4.2 Testing

The expected and actual results for maximum input torque, maximum input angle torque, and unstable equilibrium angle were compared to the predicted values, the results are shown in Table 3. The empirical values shown in Table 3 were achieved by using the test setup shown in Figure 13. A force transducer was rigidly fixed to a linear actuator, a flexible cord was then threaded through a pulley and attached to the prototype, anchored to ground at 15°. The linear actuator displaced the force transducer at a constant rate. The resulting force was obtained using Labview. The moment required to open the prototype was then calculated from the geometry.

All fatigue testing was performed using a custom fatigue testing machine. A Leeson 1 horsepower motor was used to drive a linear sled. The sled held a small ball bearing used to open and close the device, which was secured at an angle of 15°. The device was rigidly attached to ground. The motor was run at a frequency of 0.75 hertz. This frequency was selected to allow the device to open unassisted (after passing the unstable equilibrium position) and for any vibrations in

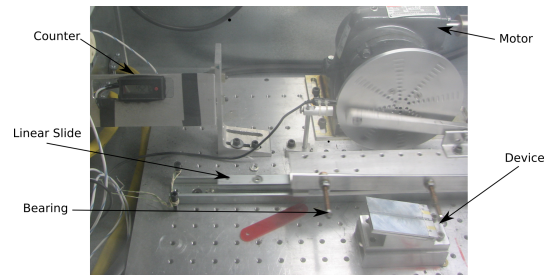


Figure 14: Components and setup of fatigue testing equipment



Figure 15: Abrasion of Kevlar fibers due to Aluminum Oxide

the upper portion of the device to dampen before the device was closed. The experimental setup is shown in Figure 14.

It is interesting to note that the main cause of failure was due to surface contact fatigue, not fatigue of the Kevlar fibers. After about two thousand cycles a black film (presumably Aluminum Oxide) appeared on the cam surfaces. It was eventually noted that the film began to flake and embed itself into the Kevlar fibers. This flaking caused the fibers to abrad, as shown in Figure 15. To prevent this problem, a small sheath was constructed by folding a thin (0.127 mm) mylar sheet and placing it around the Kevlar fibers. This prevented the majority of Aluminum Oxide from penetrating into the Kevlar, thus extending the life of the mechanism. The force required to open the device, for the sheathed prototypes, was recorded after various cycles, and these results are shown in Figure 16.

As Aluminum Oxide forms only on the outer surface (2.54 nm) of Aluminum, it is likely that the degradation of performance was due to the abrasion of the Kevlar and not the reduction in cam surface. Therefore it is believed that an entirely closed sheath, or anodization of the Aluminum, would prevent this degradation.

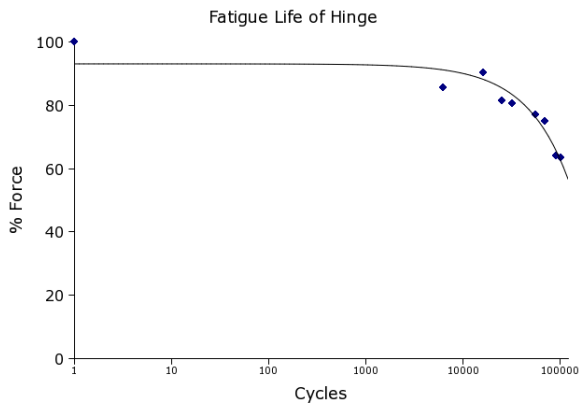


Figure 16: Percent force change with cycling of hinge

## 5 Conclusion

This paper has presented the first models of tension-based multi-stable Compliant Rolling-contact Elements. A multi-stable tension-based CORE device has been demonstrated in hardware, and the utility of the models demonstrated. The models derived in this paper were capable of producing a minimally sized hinge (6mm) capable of a fatigue life of more than 100,000 cycles, demonstrating a substantial fatigue life. Furthermore the models accurately indicated the behavior of these devices. Tension-based CORE mechanisms offer an efficient substitute for traditional pin-in-hole type joints.

## References

- [1] Howell, L., 2001. *Compliant Mechanisms*. John Wiley and Sons, Inc.
- [2] Trease, B. P., Moon, Y.-M., and Kota, S., 2005. "Design of large-displacement compliant joints". *Journal of Mechanical Design, Transactions of the ASME*, **127**(4), pp. 788 – 798.
- [3] Cannon, J. R., and Howell, L. L., 2005. "A compliant contact-aided revolute joint". *Mechanism and Machine Theory*, **40**, pp. 1273–1293.
- [4] Jeanneau, A., Herder, J., Laliberte, T., and Gosselin, C. "A compliant rolling contact joint and its application in a 3-dof planar parallel mechanism with kinematic analysis". *Proceedings of the ASME Design Engineering Technical Conference, DETC2004-57264*.
- [5] Cadman, R., 1970. "Rolamite - geometry and force analysis." Technical report, Sandia Laboratories, April.
- [6] Hilberry, B.M. and Hall, A.S., 1974 Rolling Contact Prosthetic Knee joint, *United States Patent 3,945,053*.
- [7] Cannon, J. R., Lusk, C. P., and Howell, L. L. "Compliant rolling-contact element mechanisms". *Proceedings*

*of the ASME International Design Engineering Technical Conferences and Computers and Information in Engineering Conference, DETC2005-84073*.

- [8] Mankame, N. D., and Ananthasuresh, G., 2002. "Contact aided compliant mechanisms: Concept and preliminaries". *Proceedings of the ASME Design Engineering Technical Conference*, **5 A**, pp. 109 – 121.
- [9] Mankame, N. D., and Ananthasuresh, G. K., 2004. "Topology optimization of contact-aided compliant mechanisms with smoothed contact modeling". *Computers and Structures*, **82**, pp. 1267–1290.
- [10] Mankame, N. D., 2004. "Investigations on contact-aided compliant mechanisms". Master's thesis, University of Pennsylvania.
- [11] Pellegrino, S., Kebabzade, E., Lefort, T., and Watt, A. M. 2002. "Low-Cost Hinge for Deployable Structures" Technical report, University of Cambridge.
- [12] Halverson, P. A., Magleby, S. P., Jensen, B. D., and Howell, L. L., 2007. "Concepts for achieving multi-stability in compliant rolling-contact elements". *Proceedings of the ASME International Design Engineering Technical Conferences and Computers and Information in Engineering Conference*.

